Research Article

SURFACE and INTERFACE ANALYSIS

Received: 21 December 2009 Revised: 14 July 2010 Accepted: 18 July 2010 Published online in Wiley Online Library: 25 August 2010

(wileyonlinelibrary.com) DOI 10.1002/sia.3681

The interaction of H_2O with Fe-doped $SrTiO_3$(100) surfaces

F. Voigts,[a] C. Argirusis[b,c] and W. Maus-Friedrichs[a,d]*

The interaction of H_2O with 0.013 at.% Fe-doped $SrTiO_3$(100) was investigated *in situ* with Metastable Induced Electron Spectroscopy (MIES), Ultraviolet Photoelectron Spectroscopy (UPS) and XPS at room temperature. Low Energy Electron Diffraction (LEED) was applied to gather information about the surface termination. To clear up the influence of surface defects, untreated and weakly sputtered $SrTiO_3$ surfaces were investigated. The sputtering results in the formation of oxygen-related defects in the top surface layer.

The interaction of untreated $SrTiO_3$ surfaces with H_2O is only weak. Small amounts of OH groups can be identified only with MIES due to its extreme surface sensitivity. Sputtered surfaces show a larger OH formation. Nondissociative H_2O adsorption is not observed. We therefore conclude that the exposure of H_2O to $SrTiO_3$(100) results in the dissociation near surface defects only, resulting in the formation of surface hydroxyl groups. Copyright © 2010 John Wiley & Sons, Ltd.

Keywords: MIES; UPS; XPS; LEED; strontium titanate; water

Introduction

$SrTiO_3$ has a wide-ranging field of applications, for example, as a high-temperature oxygen sensor, in photocatalysis, as substrate for high-T_c superconductors, in capacitors, and as a dielectrical component.[1–7] One reason for this wide field of applications is its remarkable thermal and chemical stability. $SrTiO_3$ is stable in a perovskite structure between 105 and 2300 K without any phase transitions and accepts very high doping concentrations. Depending on the kind and amount of doping, it shows ionic, *n*-type or *p*-type conduction. The ionic and electronic transport phenomena are frequently discussed on the basis of defect chemical descriptions.[8–10] Recently, a review by Merkle and Maier was published using Fe-doped $SrTiO_3$ as model material.[11]

One important utilization of acceptor-doped $SrTiO_3$ is its possible application as resistive high-temperature oxygen sensor, for example in the analysis of combustion engine exhausts.[12,13] The equilibrium between the surrounding oxygen partial pressure and the bulk oxygen defects, and the resulting macroscopic change of the sensor's conductivity is used as the sensor signal. The oxygen incorporation process is still a subject of some debate.[14–16] Here, the description given by Merkle and Maier is used as the basis for the discussion.

The oxygen incorporation into the sensor is dominated by the oxygen molecule dissociation probability which is determined by the Surface Density of States (SDOS) of the sensor. The oxygen dissociation is induced by an electron transfer into the antibonding $2\pi^*$ orbital of the oxygen molecule:[11,17]

$$O_2 + 2e^- \longrightarrow O_2^{2-} \longrightarrow 2O^- \quad (1)$$

The required electrons must be provided by surface states. While this is an easy process on donor-doped $SrTiO_3$, on acceptor-doped $SrTiO_3$ one bulk electronic hole per oxygen atom must be created to deliver the free electron:

$$O_2 \longrightarrow 2O^- + 2h^+ \quad (2)$$

After the molecule dissociation, the oxygen ions are temporarily adsorbed at the surface. They may be incorporated in acceptor-doped $SrTiO_3$ filling bulk oxygen vacancies through the following pathway:[11]

$$O^- + V_O^{\bullet\bullet} \leftrightarrow O_O^{\times} + h^{\bullet} \quad (3)$$

In sum, the complete reaction beginning with the impinging oxygen molecule and ending with the incorporation of an oxygen ion can be written as[11,15,18]

$$\tfrac{1}{2}O_2 + V_O^{\bullet\bullet} \leftrightarrow O_O^{\times} + 2h^{\bullet} \quad (4)$$

These processes take place in the vicinity of the $SrTiO_3$ surface and strongly depend on the SDOS. Therefore, surface analytical techniques, especially MIES, are suited best for the investigation of this important process.[19–25]

A main problem of such an oxygen sensor is its possible cross-sensitivity for other oxygen-containing gases present in the exhaust like CO, CO_2 and H_2O. According to literature,[26,27] water

* *Correspondence to: W. Maus-Friedrichs, Institut für Physik und Physikalische Technologien, Technische Universität Clausthal, Leibnizstrasse 4, 38678 Clausthal-Zellerfeld, Germany. E-mail: w.maus-friedrichs@pe.tu-clausthal.de*

a *Institut für Physik und Physikalische Technologien, Technische Universität Clausthal, Leibnizstrasse 4, 38678 Clausthal-Zellerfeld, Germany*

b *School of Chemical Engineering, National Technical University of Athens, Iroon Polytechneiou 9, Zografou 157 80, Athens, Greece*

c *Institut für Metallurgie, Technische Universität Clausthal, Robert-Koch-Str. 42, 38678 Clausthal-Zellerfeld, Germany*

d *Clausthaler Zentrum für Materialtechnik, Technische Universität Clausthal, Walther-Nernst-Str. 7, 38678 Clausthal-Zellerfeld, Germany*

is incorporated and forms OH^- ions in acceptor-doped $SrTiO_3$:

$$H_2O + V_O^{\bullet\bullet} + O_O^{\times} \leftrightarrow 2(OH)_O^{\bullet} \quad (5)$$

This was discussed by Merkle and Maier in detail.[11] The surface electronic properties, which determine the oxygen exchange coefficients, were not studied in detail up to now.

The interaction of water with undoped $SrTiO_3$(100) surfaces has been previously studied extensively, as given in the reviews of Henrich and Cox[28] and Henderson[29] in a detailed overview. It is found that no interaction with water occurs on defect-free surfaces for temperatures beyond 200 K. The introduction of defects, for example by Ar^+ bombardment, enhances the surface reactivity for water.[28–30]

On stepped $SrTiO_3$(100) surfaces also H_2O interaction is reported, resulting in the dissociation and formation of OH groups.[31,32] The OH groups were found to be bound to Ti cation sites. The authors claim that the steps are the only active sites which allow H_2O dissociation. No other surface sites, for example oxygen defects on the terraces, were able to dissociate impinging H_2O molecules.[31,32] It was assumed that adsorbed H_2O molecules diffuse over the terraces to the steps, where an immediate dissociation occurs. Afterwards, the dissociation products would diffuse back to the terrace sites forming OH bonds. In this context, the steps were acting as catalytic centers.[29,31,32]

It is the aim of this work to contribute to the understanding of the fundamental interactions of H_2O molecules with $SrTiO_3$(100) surfaces. Our investigations are not performed at the typical working temperatures of $SrTiO_3$ oxygen sensors around 1100–1300 K, because adsorption experiments are hardly feasible at these temperatures. Nevertheless, the findings will contribute to the general understanding of the surface, and thus, will be useful for the high-temperature ranges as well. Any interaction between impinging molecules and the surface at high temperatures will also occur at room temperature, possibly slowed down due to the lower thermal energy. A further work investigating the interaction with CO and CO_2 will appear soon.

Experimental

An ultrahigh vacuum (UHV) apparatus with a base pressure of 5×10^{-11} mbar, which has been described in detail previously,[33] is used to carry out the spectroscopic measurements.

Electron spectroscopy is performed using a hemispherical analyzer (VSW HA100) in combination with a source for metastable helium atoms (He^* $^3S_1$) and ultraviolet photons (HeI line). A commercial nonmonochromatic X-ray source (Specs RQ20/38C) is utilized for XPS. A commercial LEED system (Physical Electronics 11–020) is used for the investigation of the surface structure.

During XPS, X-ray photons hit the surface under an angle of 80° to the surface normal, illuminating a spot of several mm in diameter. For all measurements presented here, the Al K_α line with a photon energy of 1486.7 eV is used. Electrons are recorded by the hemispherical analyzer with an energy resolution of 1.1 eV under an angle of 10° to the surface normal. All XPS spectra are displayed as a function of binding energy with respect to the Fermi level.

For quantitative XPS analysis, photoelectron peak areas are calculated via mathematical fitting with Gauss-type profiles using OriginPro 7G including the PFM fitting module, which uses Levenberg-Marquardt algorithms to achieve the best agreement possible between experimental data and fit. Photoelectric cross-sections as calculated by Scofield,[34] and inelastic mean free paths from the NIST database,[35] as well as the transmission function of our hemispherical analyzer are taken into account when calculating stoichiometry. Details for the fitting procedure may be found in previous work.[33]

MIES and UPS are performed by applying a cold cathode gas discharge via a two-stage pumping system. A time-of-flight technique is employed to separate electrons emitted by He^* (MIES) from those caused by HeI (UPS) interaction with the surface. The combined He^*/HeI beam strikes the sample surface under an angle of 45° to the surface normal and illuminates a spot of approximately 2 mm in diameter. The spectra are recorded simultaneously by the hemispherical analyzer with an energy resolution of 220 meV under normal emission within 280 s.

MIES is an extremely surface sensitive technique probing solely the outermost layer of the sample, because the He^* atoms interact with the surface typically 0.3–0.5 nm in front of it. This may occur via a number of different mechanisms depending on surface electronic structure and work function (WF), which are described in detail elsewhere.[36–38] On $SrTiO_3$ surfaces, a special Auger Deexcitation (AD) type interaction occurs.[25] The 2s electron of the impinging He^* is resonantly transferred into the surface of the sample and localizes at near-surface Ti 3d states. Subsequently, a Ti 3d electron fills the hole in He^+ 1s in an interatomic Auger neutralization (AN) process, followed by the emission of an O 2p surface electron carrying the excess energy. The energy of the resulting MIES peak is shifted towards higher binding energies compared to conventional AD due to a diminished local ionization potential.

All MIES and UPS spectra are displayed as a function of the electron binding energies with respect to the Fermi level. The surface work function can be determined from the high binding energy onset of the MIES or the UPS spectra with an accuracy of ±0.1 eV. AD-MIES and UPS can be compared and allow a distinction between surface and bulk effects.

For all experiments, the $SrTiO_3$ is mounted in a sample manipulator by means of a molybdenum holder and introduced into the UHV as received from the supplier (Crystec GmbH Berlin, Verneuil growth method). The holder is fitted with a rearside electron bombardment heating system for the sample. Prior to the experiments, the sample is annealed at 970 K in the UHV for about 2 h, where the oxygen partial pressure is well below 10^{-13} mbar during this procedure as measured by quadrupole mass spectrometry. Only the residual gases that are commonly detected in an UHV are present: H_2, H_2O, CO and CO_2. This is done to clean the surface from adsorbates and to produce oxygen bulk vacancies $V_O^{\bullet\bullet}$. With this procedure, a sufficient number of vacancies could be produced to achieve the necessary crystal conductibility for electron spectroscopy.[19] After this initial treatment, the sample is kept under UHV conditions and is cleaned directly prior to every experiment by short annealing to about 800 K. The surfaces prepared in this manner are referred to as 'cleaned' surfaces in the following.

Sputtering of the samples is achieved by means of a Leybold-Heraus IQP 10/63 penning ion source, which is mounted in a preparation chamber directly adjacent to the analysis chamber, using argon ions as projectiles. For the sputtering procedures discussed here, ion energies of 3 keV and fluxes of about 8 μA were used. The sputter rate was identified by masking and subsequent measuring with a profilometer and amounts to about 0.008 nm s^{-1}. According to Leybold-Heraeus, the ion

beam intensity is distributed uniformly across our sample with a constant flux. The sample is treated for 300 s for all experiments, which results in a sputter depth of about 2.4 nm. All samples were cleaned prior to sputtering, as described in the preceding paragraph. Directly after sputtering, adsorbates from the residual gas in the preparation chamber are removed from the surface by cautious annealing to 560 K under the control of the MIES/UPS spectrometer. This does not remove sputter-induced defects from the surface (Fig. 7). The surfaces prepared in this manner are referred to as 'sputtered' surfaces in the following.

H_2O is offered via backfilling the chamber using a bakeable leak valve. The gas line is evacuated and can be heated in order to ensure cleanness. A quadrupole mass spectrometer (Balzers QMS 112A) is used to monitor the partial pressure of the gases during experiments simultaneously to MIES and UPS measurements.

All measurements shown here were performed at room temperature, except stated otherwise.

Results

Identification of the surface termination

$SrTiO_3$ crystals are built up by alternating SrO and TiO_2 layers in [100] direction. $SrTiO_3$(100) surfaces are mostly reported to be terminated by TiO_2 under the preparative conditions chosen here,[39] which is assumed to be due to the free surface energies.[40] In contrast, recent work reports similar free surface energies for both terminations.[41] Very recently, Wang *et al*. published an *ab initio* study taking into account surface relaxation effects as well. They also found that under vacuum conditions $SrTiO_3$(100) surfaces are terminated by a TiO_2 layer.[42] To confirm this expectation, we performed LEED measurements on our samples. Figure 1(a) shows a LEED image of the cleaned $SrTiO_3$(100) surface, the primary electron energy is 97 eV. A clear diffraction pattern can be detected. Figure 1(b) shows the schematic representation of the observed LEED spots. It is recognizable, that the observed diffraction image is due to a 1×1 surface. It is similar to the LEED results published by Tanak *et al*., who annealed their $SrTiO_3$(100) surfaces at 870 K.[43] We conclude, therefore, in a first step, that under the preparative conditions chosen here a nonreconstructed clean $SrTiO_3$(100) surface appears. Owing to the clear diffraction pattern, a long-range order of the surface atoms must be present.

The MIES spectrum of the $SrTiO_3$(100) surfaces (given in the next section) can only be understood assuming a TiO_2 termination of the $SrTiO_3$(100) surface. In a previous work, we discussed the structure of the MIES spectrum of $SrTiO_3$(100) on the basis of *ab initio* calculations in detail.[25] We could show, that the interaction between the impinging He^* and the $SrTiO_3$ is fundamentally based on the availability of reduced Ti 3d states in resonance with the He 2s orbital at the surface. On a SrO-terminated surface, this would not be the case, and therefore, the MIES spectra would look quite different. In an unpublished work on the same apparatus, we obtained MIES spectra from SrO surfaces that do evidence this. Furthermore, the MIES spectrum obtained here appears to be very similar to the ones obtained for TiO_2 surfaces.[44]

Our own previous measurements on these surfaces showed that after the preparation applied here a clear Ti and O enrichment on top of the surface is found.[24,45] This was shown by AES of the top surface layers as well as with AES depth profile analysis. In addition, we found microscopically, that the $SrTiO_3$ surface displays reconstructions consisting of TiO_2 microfacets.[24]

Taking into account all these observations and all mentioned indications we conclude that the $SrTiO_3$(100) surface investigated here is at least mainly terminated by a TiO_2 layer. We will give more arguments for this result with the discussion of the MIES results.

Spectroscopic results

Figure 2 shows MIES (a) and UPS (b) spectra of the cleaned $SrTiO_3$(100) surface. The bottom spectrum corresponds to the cleaned surface, the spectra obtained during the interaction with water are shown in a waterfall manner, the top spectrum corresponds to the surface saturated with 1250 L of water. Besides the secondary electron emission appearing beyond binding energies of $E_B = 12$ eV, MIES shows one peak at $E_B = 6.7$ eV, while UPS shows a peak doublet at $E_B = 5.0$ and 7.2 eV. It has been published previously, that the MIES peak at $E_B = 6.7$ eV as well as the UPS peak at $E_B = 5.0$ eV arise from the ionization of nonhybridized O 2p atomic orbitals, while the UPS peak at $E_B = 7.2$ eV arises from O 2p-Ti 3d hybridized orbitals.[25] MIES shows only one peak, because the nonhybridized O 2p atomic orbitals protrude much wider into the vacuum than all other wave functions. Therefore, the impinging metastable He^* atoms can only interact with these wave functions. For UPS, which provides

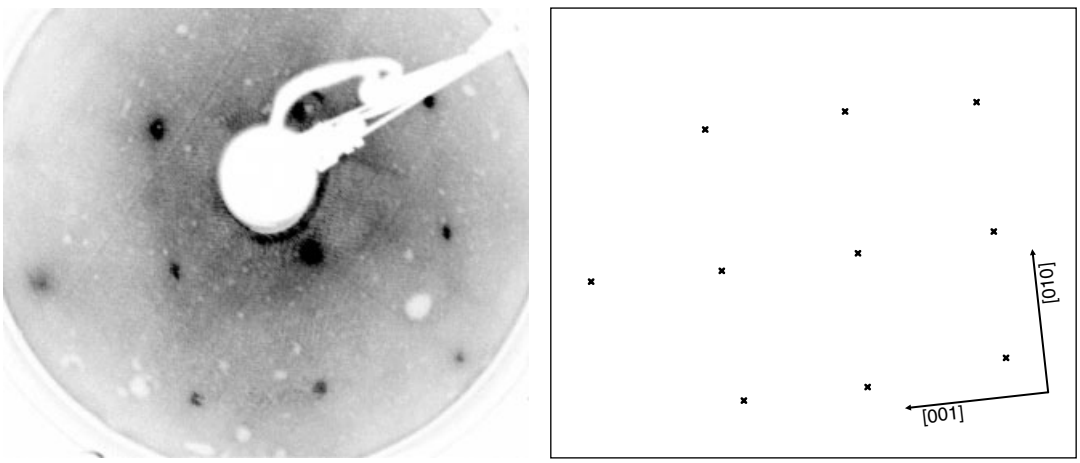

Figure 1. LEED image (a) and schematic representation of the observed spots (b) of the cleaned $SrTiO_3$(100) surface; primary electron energy is 97 eV.

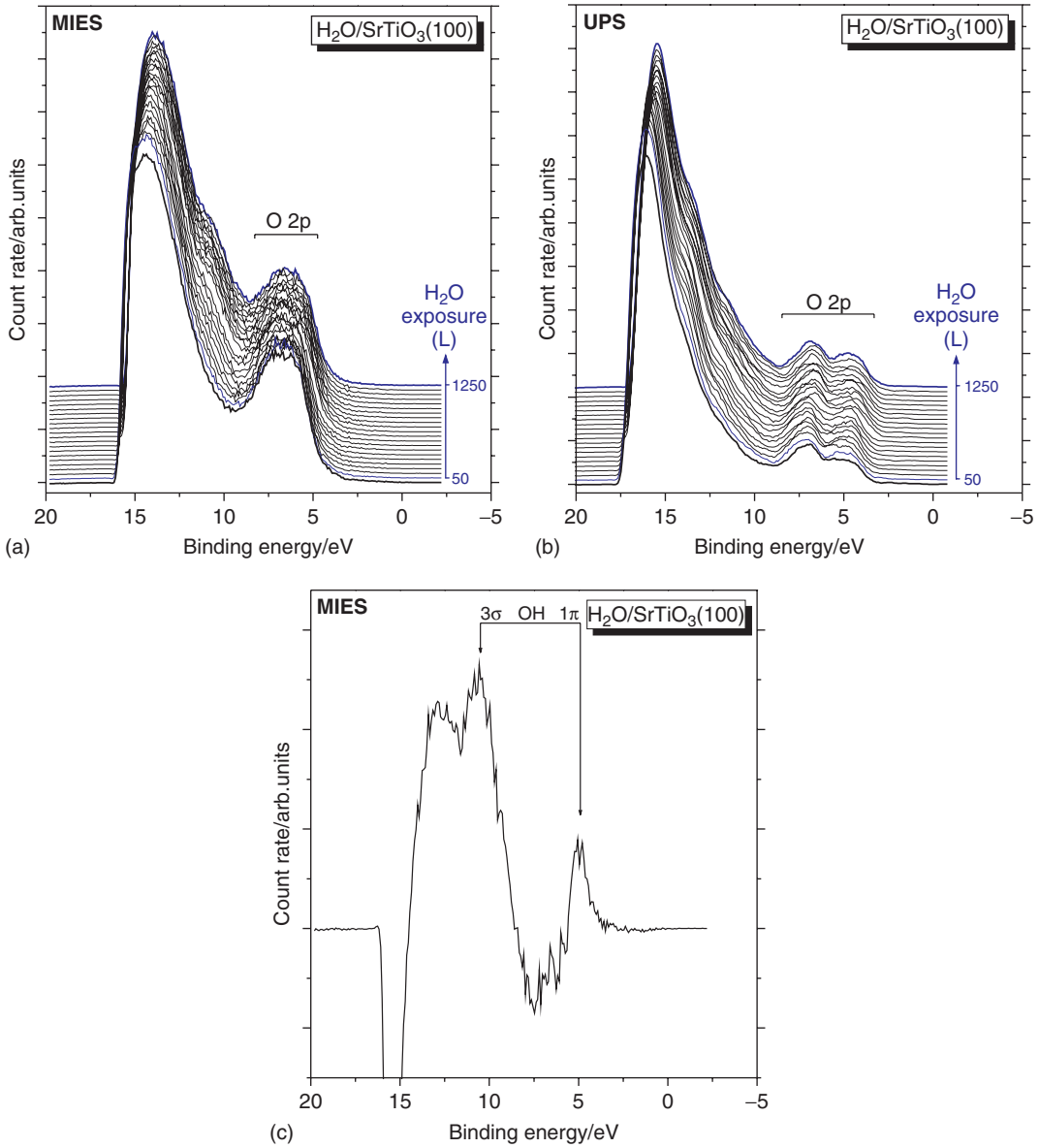

Figure 2. MIES (a) and UPS (b) spectra of cleaned $SrTiO_3(100)$ during H_2O exposure; difference spectrum between top and bottom MIES spectrum (c).

an information depth of 1–2 nm typically, this is not the case. In MIES, the He* 2s electron is transferred into the sample surface localizing near a Ti 3d state. Subsequently, a Ti 3d electron fills the hole in the He^+ 1s in an interatomic AN process followed by the emission of an O 2p surface electron carrying the excess energy.[25] The resulting spectra are, in principle, very similar to AD spectra, but the binding energy of the MIES spectra is shifted to higher energies by 1.7 eV and the O 2p peak is broadened.

This interaction process is only possible when unoccupied Ti 3d states are available in resonance with the He 2s orbital of the impinging He* atoms. This would not be the case if the surface would be terminated by a SrO layer. On a SrO-terminated surface, the MIES spectrum would be due to a conventional AD process and the O 2p peak would be much sharper and show a distinct shoulder at about 2 eV higher binding energy besides the peak maximum, which is not observed here. Quite the contrary, the spectrum is very similar to spectra obtained on TiO_2 surfaces.[44] These findings support the conclusions in our earlier section.

With increasing H_2O exposure, the work function increases slightly. A new weak peak appears around $E_B = 10.5$ eV, and the O 2p emission appears to become broader on the left side. To gather further information, we performed a difference spectrum of the MIES spectra of the cleaned and the water saturated surface. This was done without any rescaling or other manipulation, but only by plain subtraction of the respective count rates. The result is shown in Fig. 2(c). A peak doublet is found at $E_B = 5.0$ and 10.6 eV. This is due to the OH formation which is known to show such a doublet deriving from the 1π and 3σ molecular orbitals (MO).[46] The adsorption of H_2O molecules would lead to a well known peak triplet at $E_B = 8.0$, 10.2 and 14.1 eV.[47] We can exclude that for this experiment.

XPS results for the cleaned, water saturated Fe-doped $SrTiO_3(100)$ surface are presented in Fig. 3. The survey spectrum (a) shows $SrTiO_3$ in its stoichiometric composition. The small peaks corresponding to Mo result from electron emission from the sample holder. They do neither disturb the measurements nor do they

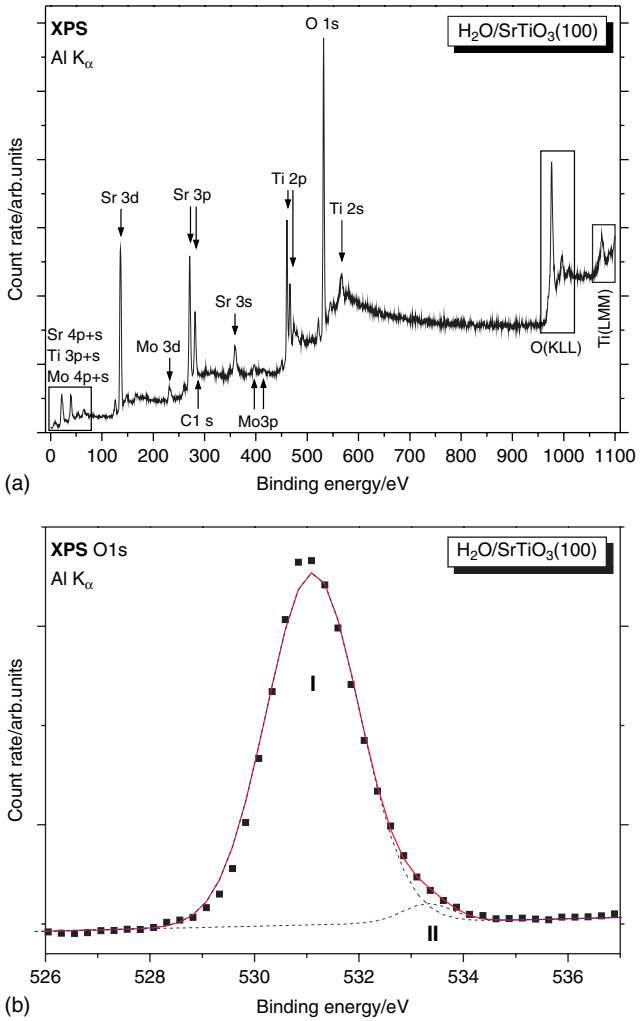

Figure 3. XPS spectra of cleaned, H_2O saturated $SrTiO_3(100)$: survey spectrum (a) and O 1s region (b).

have any influence on the results. Contributions of Fe are not found because the doping concentration of 0.013 at.% is lower than the detection limit of our XPS system. A mathematical analysis using Gauss-type functions of the O 1s regions is shown in Fig 3(b). The dots present the raw data, the dashed blue lines show the two contributions from the main peak I and the satellite peak II, the solid red line shows the sum of them. O 1s shows a main peak I at $E_B = 531.1$ eV with a Full Width at Half Maximum (FWHM) of 2.1 eV. It is accompanied by a small peak II at $E_B = 533.3$ eV with a FWHM of 1.1 eV. Peak I arises from ionization of lattice oxygen[48] (from regular $O_O^{\times}$ sites) while peak II must be due to a second species, its relative contribution amounts to 2.7% of the total O 1s signal. This secondary contribution is also observed on cleaned surfaces without water exposure.

The Sr 3d and Ti 2p regions do not show any contributions besides the main peaks for regular lattice strontium and lattice titanium. They remain unchanged by any water exposure of the sample, which is in agreement with literature for TiO_2-terminated surfaces.[49]

Figure 4 shows MIES (a) and UPS (b) spectra of the Ar^+ sputtered $SrTiO_3(100)$ surface. The bottom spectra correspond to the sputtered surface, the spectra obtained during the interaction with water are shown in a waterfall manner, the top spectra correspond to the surface saturated with 224 L of water. Again, besides the secondary electron emission beyond binding energies $E_B = 12$ eV, MIES of the unexposed surface shows one peak at $E_B = 6.7$ eV, while UPS shows a peak doublet at $E_B = 5.0$ and 7.2 eV. With increasing H_2O exposure the work function increases and a peak doublet in MIES appears at $E_B = 6.4$ and 11.2 eV. This is the well known characteristic of a OH formation.[46] The adsorption of H_2O can again be excluded.

UPS shows almost no changes. We produced difference spectra between sputtered and water-saturated $SrTiO_3$ like the one for MIES in Fig. 2(c). None of these spectra did show any recognizable features. Such behavior has been observed previously. On CaO surfaces, we observed a large number of OH molecules with MIES, while UPS showed only very small traces of these surface OH groups by contrast.[46] Thus we can conclude, that OH formation occurs on the sputtered $SrTiO_3(100)$, but is restricted to the surface and covers a small number of locations on top of the surface only.

The XPS results in Fig. 5 show the water-saturated sputtered Fe-doped $SrTiO_3(100)$ surface. The survey spectrum (a) shows $SrTiO_3$ in its stoichiometric composition. Compared to cleaned $SrTiO_3$ (Fig. 3), the oxygen content is reduced by about 1 at.%, while the titan content is raised by about 1 at.%. The strontium contributions remains the same, approximately. Again, the sample holder contributions do not disturb the measurements and do not have any influence on the results. The detail analysis of the O 1s region in Fig. 5(b) shows a main peak at $E_B = 530.8$ eV with a FWHM of 2.1 eV. It is accompanied by a small second peak at $E_B = 533.0$ eV with a FWHM of 1.3 eV. The relative contribution of this peak amounts to 4.6% of the total O 1s signal.

Work function change and OH formation rate as a function of the H_2O exposure from the MIES spectra in Fig. 4 are plotted in Fig. 6. The OH formation is evaluated by analyzing the OH 3σ emission, and the work function is evaluated by the low energy onset of the MIES spectra. The work function increases by about 0.5 eV, and the OH formation increases with the H_2O exposure. Work function and OH 3σ emission are linearly related. The work function change of the cleaned surface from Fig. 2 is drawn for comparison. Similarly, also for the OH formation on CaO, we found a work function increase of about 0.5 eV and a linear relation between OH formation and work function increase.[46]

Figure 7 shows MIES spectra of the band gap between the Fermi level and $E_B = 5$ eV. The Fermi level is pinned to the conduction band, the gap width of about 3 eV corresponds to previous findings.[21–25] The top spectrum shows the surface directly after sputtering. This surface is slightly contaminated from residual gas components which are desorbed at a temperature of 560 K. After this smooth cleaning procedure, contribution from surface defects in the band gap appear around 0.9 eV below the Fermi level. These states in the band gap are well known oxygen defects which result in the occupation of surface Ti 3d orbitals.[21–23,31,32]

Heating at 620 K removes these defect states completely. This cannot be induced by adsorption processes from the residual gas in the vacuum, because the base pressure, which is below 5×10^{-9} mbar (>90% He) during MIES measurements, is too low. Furthermore, this would have already happened at even lower temperatures.

Discussion

The interaction of H_2O with cleaned $SrTiO_3(100)$ surfaces results in the formation of OH groups from partial H_2O dissociation on top of

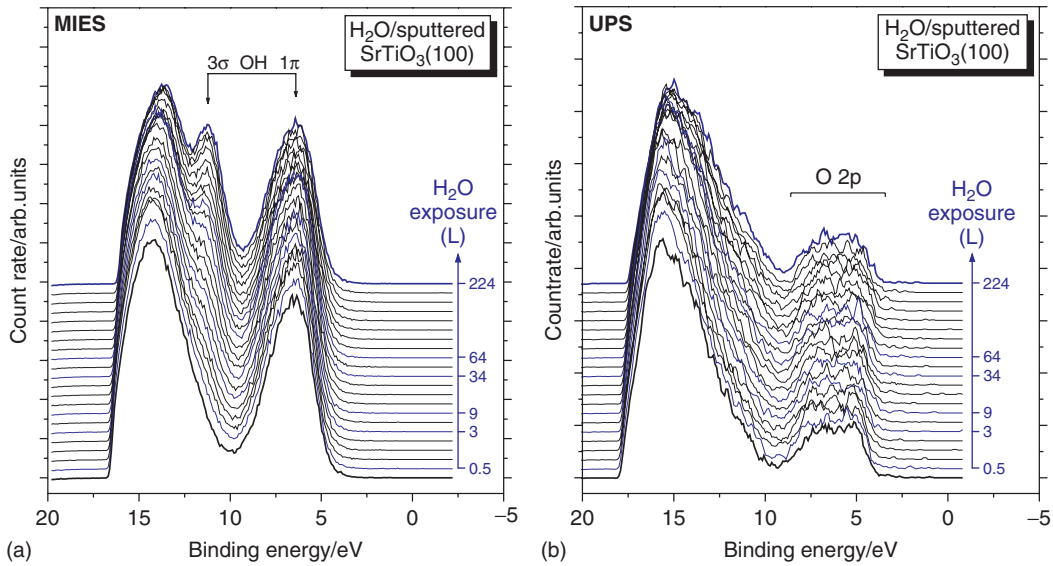

Figure 4. MIES (a) and UPS (b) spectra of sputtered $SrTiO_3(100)$ during H_2O exposure.

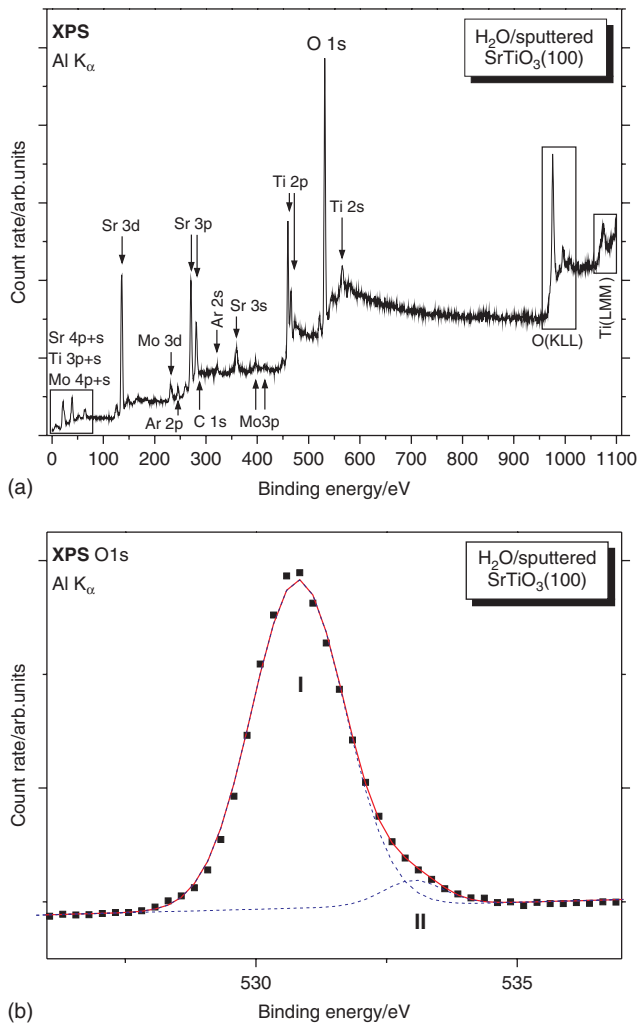

Figure 5. XPS spectra of H_2O saturated sputtered $SrTiO_3(100)$: survey spectrum (a) and O 1s region (b).

the surface. H_2O adsorption does not occur at all. The comparison of MIES and UPS (Fig. 2) shows, that the amount of OH is very low and that the interaction probability is weak. It takes about 1250 L of H_2O to achieve saturation. In MIES we find only a very small amount of OH and no traces in UPS. The XPS results of the O 1s region show a small peak at higher binding energies which we attribute to surface defects. These defects are also detected on the cleaned surface not exposed to water. Additional contributions from OH groups are not detected because there are too few of them at the surface to be detectable with our XPS setup. We therefore assume that the dissociation of impinging H_2O may only occur at these defect sites and that the dissociation probability is low. The adsorption of OH resulting from this dissociation process appears to be possible only on such defects as well. Density functional theory calculations indicate that defect surface sites are important for this adsorbate–surface reactivity.[48] The distance between the OH 1π and 3σ molecular orbitals amounts to 5.6 eV. This is larger than for OH groups on other systems. Measured with MIES we found distances of 3.9 eV for $Sr(OH)_2$ surface layers[50] and 4.2 eV for $Ca(OH)_2$ layers[46] for example. Similar behavior has been described previously:[29,31,32] most probably the 3σ orbital is stabilized by an additional interaction with surface orbitals because the OH is not oriented perpendicular to the surface but slightly tilted. This causes the observed change in binding energy difference.

Sputtering of the $SrTiO_3(100)$ surfaces does change the surface electronic structure significantly. On the sputtered surfaces, no LEED pattern may be observed anymore. This is obviously due to the loss of the long-range ordering of the surface. Even after adsorption of water or a short annealing to 800 K, the LEED pattern remains absent. To restore it, annealing at 970 K for about half an hour is necessary.

The sputtering process changes the MIES and UPS spectra, too. In MIES, the O 2p peak at $E_B = 6.7$ eV increases during sputtering, otherwise the spectrum remains unchanged. Especially, no change in the He* deexcitation process may be observed. This indicates the continued presence of unoccupied Ti 3d states at the surface. Thus, the TiO_2 termination of the surface seems to be preserved during the sputtering process.

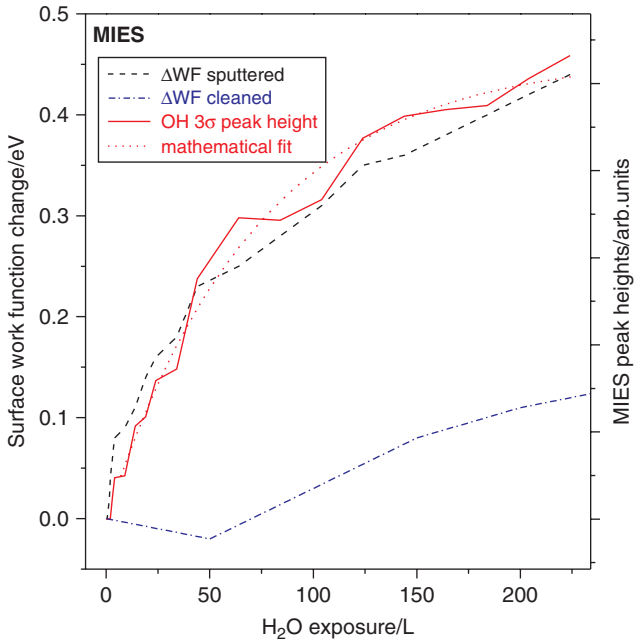

Figure 6. OH peak growth and work function change during H_2O exposure of the sputtered $SrTiO_3(100)$ surface accompanied by a mathematical fit, work function change of the cleaned surface is drawn for comparison.

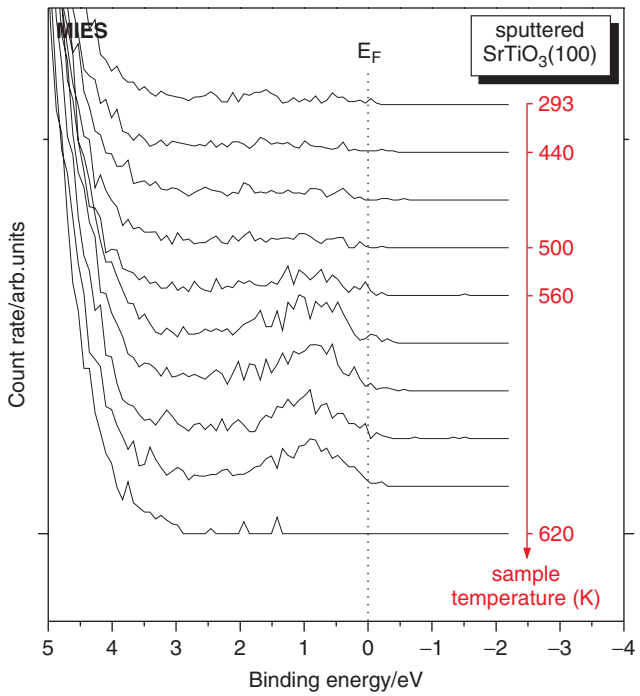

Figure 7. Defects in the band gap of $SrTiO_3$ directly after sputtering observed with MIES as a function of sample temperature.

In UPS, the peak at $E_B = 5.0$ eV (due to ionization of nonhybridized O 2p orbitals) increases while the peak at $E_B = 7.2$ eV (due to ionization from O 2p-Ti 3d hybridized orbitals) decreases correspondingly. This can be seen from the comparison of the respective bottom spectra in Figs 2 and 4. This means, that the sputtering reduces the number of O 2p-Ti 3d hybridized orbitals in the surface remarkably while the number of nonhybridized O 2p orbitals increases realtively. It is known from literature[51] that oxygen is preferentially desorbed during sputtering from $SrTiO_3(100)$ surfaces. Furthermore, we find that the work function of the cleaned surface decreases by 0.7 eV during sputtering. This may, on the one hand, be due to the Smoluchowksi effect described for metals,[52] where even small roughening results in a remarkable work function decrease. On the other hand, the oxygen desorption may result in the decrease of surface dipoles, thus decreasing the lateral work function. Taking into account all mentioned observations, we conclude that during sputtering preferentially oxygen is desorbed. This conclusion is backed up by our global XPS spectra, which show a slight decrease in oxygen content and a small increase in titanium content after sputtering the surface.

XPS shows a minor O 1s peak with a relative contribution of 2.7% for the cleaned and 4.6% for the sputtered surface. We assume that this minor peak is related to surface defects. We know from the LEED results, that the long-range ordering of the surface is destroyed by the sputtering process, and from the MIES and the global XPS results we know that oxygen is desorbed by it preferentially. It is reasonable to conclude, that sputtering the surface results in the breaking of Ti–O bonds. This may result in the desorption of oxygen and the production of $V_O^{\bullet\bullet}$ and/or undercoordinated surface oxygen atoms. We expect that these undercoordinated atoms are visible with XPS as the minor O 1s peak.

If one assumes that these undercoordinated atoms are restricted to the surface layer of the $SrTiO_3(100)$, we estimate that about one quarter of the oxygen atoms in the sputtered surface are defective. This estimation is drawn from the calculation of inelastic mean free paths[35] of the respective electrons in $SrTiO_3$ and the application of a simple exponential decay law. This gives an estimate of how much the first $SrTiO_3$ layer contributes to the total XPS signal. We assume that H_2O dissociation and OH formation only take place at defect sites. Again, no additional contribution is detected in XPS when the surface is exposed to water.

The H_2O interaction with the sputtered surfaces again results in the formation of OH bonds restricted to the top of the surface. The amount of OH is larger than for the unsputtered surface but we are not able to give any values on the basis of the MIES and UPS measurements. In any case, the coverage is well below a full monolayer, since the features in MIES are way too small for that, and because UPS does not show any OH formation. On the basis of our previous works for the OH formation on CaO[46] and SrO[50] surfaces, we assume that the number of OH groups on the surface detected by MIES, and the number of surface defects detected with XPS may coincide. The reaction probability must be very low, because more than 200 L are required to saturate these defects with OH groups.

The OH formation on the sputtered surface, shown in Fig. 6, can be fitted by a simple Langmuir-type isotherm (dotted line) in the form $\theta = 1 - \exp(-S_0\ \Gamma\ t)$, where θ is the relative coverage of the surface defects with OH groups, S_0 is the reaction probability and Γ is the number of H_2O molecules impinging per surface defect and second. Unfortunately, we neither know S_0 nor Γ quantitatively. Thus, we cannot calculate reaction probabilities from the fit. We found similar behavior for the OH formation on CaO.[46] This means that the interaction process must follow the simple scheme described above: impinging H_2O molecules are dissociated at surface defect sites and the resulting OH is adsorbed at the surface defect. This does not follow the picture mentioned by Thornton and coworkers,[31,32] that the dissociation

is performed at catalytic-active sites, and that the OH adsorption may occur on all surface sites. The work function changes linearly with the OH formation. This means, that the work function change is only a function of the number of adsorbed OH dipoles on top of the surface. Because this linearity holds up to H_2O saturation, no dipol–dipol interaction must be taken into account for the WF change. Therefore, the OH coverage must be only small.

The detailed spectra in Fig. 7 show, that defect states may be observed obviously in the band gap of sputtered $SrTiO_3$(100) only with MIES. They correspond to Ti 3d states located just below the Fermi level, which has been observed for donor-doped $SrTiO_3$ surfaces with MIES previously.[21–23] Such defects are not observed before sputtering. This backs up the conclusion, that the sputtering process results in the breaking of surface Ti–O bonds. The electron count rate in this part of the MIES spectrum is extremely low, about two orders of magnitude lower than for the other structures discussed here. This is why they are not observed in the other MIES spectra. Furthermore, the detection of these states depends crucially on the soft cleaning procedure described in the Experimental section.

These surface states vanish at temperatures around 620 K. Comparable observations have been reported previously.[53] The features from OH 1π and OH 3σ MOs in MIES have vanished at these temperatures due to desorption of the OH groups into the vacuum. Because of the very low residual gas pressure below 5×10^{-10} mbar during our MIES measurements, a saturation with other gas components is impossible. Additionally, no hint of other adsorbates can be detected in MIES or UPS at this state. We must therefore conclude that the surface defects are occupied by oxygen atoms from the $SrTiO_3$ bulk crystal.

Furthermore, the minor peak observed in the O 1s region with XPS is significantly reduced by annealing the sample to 620 K (not shown here). Prolonged annealing returns the relative contribution to the state before sputtering. These observations give a strong hint, that the oxygen defect mobility is sufficiently high even at 620 K.

Additional water-exposure experiments (not shown here) in the manner discussed with Fig. 4 reveal that the Ti 3d surface defect states are also removed by the adsorption of surface OH groups.

Concerning the nature of the sputter-induced surface defects, there are several observations to consider. The sputtering of the $SrTiO_3$(100) surface manifests itself in six respects: (i) in the loss of the long-range ordering of the surface as detected with LEED; (ii) in the increase of the peak due to ionization of nonhybridized O 2p orbitals in UPS, while the peak due to ionization from O 2p-Ti 3d hybridized orbitals decreases correspondingly; (iii) in the development of reduced Ti 3d states in the band gap that may be observed with MIES; (iv) in the increase of the minor XPS O 1s peak from 2.7 to 4.6% of the total O1s signal; (v) in a slight decrease in global oxygen content and a small increase in global titanium content; and (vi) the enhanced reactivity of the surface to hydroxyl group formation from water.

From all this, it is reasonable to conclude that the main consequence of sputtering the surface is the breaking of surface Ti–O bonds. Possibly, the defects created by this are of two different kinds: surface oxygen defects $V_O^{\bullet\bullet}$ and undercoordinated oxygen and titanium atoms. The global XPS results hint to $V_O^{\bullet\bullet}$ and the XPS O 1s results to undercoordinated oxygen atoms. The MIES/UPS findings and the enhanced surface reactivity may be due to both types of defects. Further experiments are required to clear this up. Hence, the nature of the observed surface defects and their role in the reaction with water is still under investigation.

Our experiment gives no information for a possible total dissociation into single H and O atoms happening in the vicinity of the of the $SrTiO_3$(100) surface because these atoms would most likely not be detected with our spectroscopic techniques. Hence, we cannot exclude total dissociation of H_2O molecules at the surface that may provide an oxygen atom source for incorporation processes into the crystal. We will address this in a forthcoming study.

Conclusion

MIES, UPS, XPS and LEED were applied to study the interaction of H_2O with Fe-doped $SrTiO_3$(100) surfaces. To gather insight in the interaction process, cleaned and sputtered $SrTiO_3$ surfaces were investigated. The $SrTiO_3$ is always at least mainly terminated by a TiO_2 layer under the preparative conditions used here. Sputtering results in the breaking of Ti–O bonds at the surface and the formation of surface defects.

The interaction of H_2O molecules with these surfaces only occurs on surface defect sites. Obviously, partial dissociation of the impinging H_2O and adsorption of OH on top of the surface takes place at the same sites. No hints for any catalytic reaction were found. The OH coverage for the sputtered $SrTiO_3$(100) surface appears to amount to about one quarter. For the cleaned surface, this is much less. Neither UPS nor XPS give any information about the OH formation, which is in contrast very well visible with MIES.

Sputtering produces defects which are visible in MIES as reduced Ti 3d states within the band gap. These defects are similar to previously observed ones for donor-doped $SrTiO_3$ surfaces heated under vacuum conditions. These defect states are cured by oxygen atoms from internal diffusion processes even at 620 K.

For its possible application as a high-temperature oxygen sensor at temperatures beyond 1000 K this implies interesting questions. The impinging H_2O molecules are only dissociated at defects sites and are bound only weakly. Even heating at 560 K removes any OH groups completely. However, total dissociation and incorporation of oxygen from water cannot be excluded.

Acknowledgements

The financial supports by the Deutsche Forschungsgemeinschaft under contract Nos Ma 1893/9 and Ar 248/3 are gratefully acknowledged. The authors gratefully acknowledge the technical assistance of Sebastian Dahle.

References

[1] B. Stäuble-Pumpin, B. Ilge, V. C. Matjasevic, P. M. L. O. Scholte, A. J. Steinfort, F. Tuinstra, *Surf. Sci.* **1996**, *369*, 313.
[2] Y. Liang, D. A. Bonnell, *Surf. Sci.* **1994**, *310*, 128.
[3] V. Ravikiumar, D. Wolf, P. David, *Phys. Rev. Lett.* **1995**, *74*, 174.
[4] K. Szot, W. Speier, *Phys. Rec. B* **1999**, *60*, 5909.
[5] K. Szot, W. Speier, U. Breuer, R. Meyer, J. Szade, R. Waser, *Surf. Sci.* **2000**, *460*, 112.
[6] R. Moos, T. Bischoff, W. Menesklou, K. H. Härdtl, *J. Mat. Sci.* **1997**, *32*, 4247.
[7] S. Steinsvik, R. Bugge, J. Gjønnes, J. Taftø, T. Norby, *J. Phys. Chem. Sol.* **1997**, *58*, 969.
[8] G. M. Choi, H. J. Tuller, *J. Am. Ceram. Soc.* **1988**, *71*, 201.
[9] R. Moos, K. H. Härdtl, *J. Am. Ceram. Soc.* **1997**, *80*, 2549.
[10] N. H. Chan, R. K. Sharma, D. M. Smyth, *J. Electrochem. Soc.* **1981**, *128*, 1762.
[11] R. Merkle, J. Maier, *Angew. Chem. Int. Ed.* **2008**, *47*, 2.

[12] W. Menesklou, H. J. Schreiner, K. H. Härdtl, E. Ivers-Tiffée, *Sens. Actuators B* **1999**, *59*, 184.
[13] R. Mayer, R. Waser, *Sens. Actuators B* **2004**, *101*, 33.
[14] Chr. Argirusis, S. Wagner, W. Menesklou, C. Warnke, T. Damjanovic, G. Borchardt, E. Ivers-Tiffee, *PCCP* **2005**, *7*, 3523.
[15] M. Leonhardt, R. A. de Souza, J. Claus, J. Maier, *J. of the Electrochem. Soc.* **2002**, *149*, J19.
[16] R. A. de Souza, M. Martin, *PCCP* **2008**, *10*, 2356.
[17] A. Zangwill, *Physics at Surfaces*, Cambridge University Press, Cambridge, **1989**.
[18] S. B. Adler, X. Y. Chen, J. R. Wilson, *Journal of Catalysis* **2007**, *245*, 91.
[19] Chr. Argirusis, F. Voigts, P. Datta, J. Grosse-Brauckmann, W. Maus-Friedrichs, *Phys. Chem. Chem. Phys.* **2009**, *11*, 3152.
[20] F. Voigts, T. Damjanovic, G. Borchardt, Chr. Argirusis, W. Maus-Friedrichs, *Journal of Nanomaterials* **2006**, Article ID 63154.
[21] A. Gömann, K. Gömann, M. Frerichs, V. Kempter, G. Borchardt und W. Maus-Friedrichs, *Appl. Surf. Sci.* **2005**, *252*, 196.
[22] A. Gunhold, K. Gömann, L. Beuermann, V. Kempter, G. Borchardt, W. Maus-Friedrichs, *Surf. Sci.* **2004**, *566*, 105.
[23] A. Gunhold, L. Beuermann, K. Gömann, G. Borchardt, V. Kempter, W. Maus-Friedrichs, S. Piskunov, E. A. Kotomin, S. Dorfman, *Surf. Int. Anal.* **2003**, *35*, 998.
[24] A. Gunhold, L. Beuermann, M. Frerichs, V. Kempter, K. Gömann, G. Borchardt, W. Maus-Friedrichs, *Surf. Sci.* **2003**, *523*, 80.
[25] W. Maus-Friedrichs, M. Frerichs, A. Gunhold, S. Krischok, V. Kempter, G. Bihlmayer, *Surf. Sci.* **2002**, *515*, 499.
[26] K. D. Kreuer, *Solid State Ionics* **1999**, *125*, 285.
[27] J. H. Yu, J.-S. Lee, J. Maier, *PCCP* **2005**, *7*, 3560.
[28] V. E. Henrich, P. A. Cox, *The Surface Science of Metal Oxides*, Cambridge University Press, Cambridge, **1989**.
[29] M. A. Henderson, *Surf. Sci. Rep.* **2002**, *46*, 1.
[30] C. Webb, M. Lichtensteiger, *Surf. Sci. Lett.* **1981**, *107*, L345.
[31] N. B. Brookes, G. Thornton, F. M. Quinn, *Sol. State Comm.* **1987**, *64*, 383.
[32] N. B. Brookes, F. M. Quinn, G. Thornton, *Vacuum* **1988**, *38*, 405.
[33] M. Frerichs, F. Voigts, W. Maus-Friedrichs, *Appl. Surf. Sci.* **2006**, *253*, 950.
[34] J. H. Scofield, *J. Electron Spectr. Rel. Phenom.* **1976**, *8*, 129.
[35] National Institute of Standards and Technology, *Electron Inelastic-Mean-Free-Path Database 1.1*, http://www.nist.gov/srd/nist71.htm.
[36] Y. Harada, S. Masuda, H. Ozaki, *Chem. Rev.* **1997**, *97*, 1897.
[37] H. Morgner, *Adv. Atom. Mol. Opt. Phys.* **2000**, *42*, 387.
[38] G. Ertl, J. Küppers, *Low Energy Electrons and Surface Chemistry*, VCH Verlag, Weinheim, **1985**.
[39] A. D. Polli, T. Wagner, T. Gemming, M. Rühle, *Surf. Sci.* **2000**, *448*, 279.
[40] P. A. W. van der Heide, Q. D. Jiang, Y. S. Kim, J. W. Rabalais, *Surf. Sci.* **2001**, *473*, 59.
[41] R. A. Evarestov, A. V. Bandura, V. E. Alexandrov, *Surf. Sci.* **2007**, *601*, 1844.
[42] G.-Z. Wang, C.-R. Li, J. Cui, Z.-Y. Man, *Surf. Interf. Anal.* **2009**, *41*, 918.
[43] Y. Tanaka, H. Morishita, M. Watamori, K. Oura, I. Katayama, *Appl. Surf. Sci.* **1994**, *82/83*, 528.
[44] S. Krischok, J. A. Schaefer, O. Höfft, V. Kempter, *Surf. Interf. Anal.* **2004**, *36*, 83.
[45] A. Gunhold, K. Gömann, L. Beuermann, M. Frerichs, G. Borchardt, V. Kempter, W. Maus-Friedrichs, *Surf. Sci.* **2002**, *507-510*, 447.
[46] F. Bebensee, F. Voigts and W. Maus-Friedrichs, *Surf. Sci.* **2008**, *602*, 1622.
[47] S. Krischok, O. Höfft, J. Günster, J. Stultz, D. W. Goodman, V. Kempter, *Surf. Sci.* **2001**, *495*, 8.
[48] J. D. Baniecki, M. Ishii, K. Kurihara, K. Yamanaka, T. Yano, K. Shinozaki, T. Imada, Y. Kobayashi, *J. Appl. Phys.* **2009**, *106*, 054109.
[49] K. Iwahori, S. Watanabe, M. Kawai, *J. Appl. Phys.* **2003**, *93*, 3223.
[50] W. Maus-Friedrichs, A. Gunhold, M. Frerichs, V. Kempter, *Surf. Sci.* **2001**, *488*, 239.
[51] A. Hirata, A. Ando, K. Saiki, A. Koma, *Surf. Sci.* **1994**, *310*, 89.
[52] R. Smoluchowski, *Phys. Rev.* **1941**, *60*, 661.
[53] A. Hirata, A. Ando, K. Saiki, A. Koma, *Surf. Sci.* **1994**, *310*, 89.